Available online at www.sciencedirect.com
SCIENCE DIRECT®
International Journal of Heat and Mass Transfer 49 (2006) 3221–3228
International Journal of HEAT and MASS TRANSFER
www.elsevier.com/locate/ijhmt

Entropy generation in natural convection in a symmetrically and uniformly heated vertical channel

Assunta Andreozzi [a], Antonio Auletta [b], Oronzio Manca [c,*]

[a] Dipartimento di Energetica, Termofluidodinamica applicata e Condizionamenti ambientali, Università degli Studi di Napoli Federico II, Piazzale Tecchio 80, 80125 Napoli, Italy
[b] CIRA – Centro Italiano Ricerche Aerospaziali, Via Maiorise 1, 81043 Capua (CE), Italy
[c] Dipartimento di Ingegneria Aerospaziale e Meccanica, Seconda Universitá degli Studi di Napoli, Real Casa dell'Annunziata, Via Roma 29, 81031 Aversa (CE), Italy

Received 29 July 2005
Available online 30 March 2006

Abstract

In this study numerical predictions of local and global entropy generation rates in natural convection in air in a vertical channel symmetrically heated at uniform heat flux are reported. Results of entropy generation analysis are obtained by solving the entropy generation equation based on the velocity and temperature data. The analyzed regime is two-dimensional, laminar and steady state. The numerical procedure expands an existing computer code on natural convection in vertical channels. Results in terms of fields and profiles of local entropy generation, for various Rayleigh number, Ra, and aspect ratio values, L/b, are given. The distributions of local values show different behaviours for the different Ra values. A correlation between global entropy generation rates, Rayleigh number and aspect ratio is proposed in the ranges $10^3 \leqslant Ra \leqslant 10^6$ and $5 \leqslant L/b \leqslant 20$.

Keywords: Entropy generation; Numerical analysis; Vertical channel; Natural convection

1. Introduction

The optimal design criteria for thermal systems by minimizing their entropy generation have recently been a topic of great interest in the fields related to thermal power plants, heat exchangers, energy-storage systems, and electronic cooling devices [1,2]. In these criteria, the total entropy generation in the designed systems can be minimized under some physical and geometric arrangements, and an optimal configuration with minimum loss of available energy may be obtained [2]. Analytical procedures for evaluating local entropy generation and thermal optimization were summarized in [2,3] and many applications have been carried out to fluid flows with analytical solutions for the velocity and temperature fields as for example in [4–15].

Inclusion of entropy generation calculations in computational fluid dynamics codes would allow the evaluation of local entropy generation in more complicated thermal phenomena as remarked in [16]. One theoretically correct measure of thermodynamic performance is the magnitude of thermodynamic irreversibilities associated with a component or process. It can be shown that the minimization of entropy generation also results in the maximum reduction of irreversibility (see for example [2]). The development of improved thermal designs is enhanced by the ability to identify clearly the source and location of entropy generation.

Systems of individual components can be optimized by estimating the net entropy generation for complete components, but the development of novel components and processes should benefit from knowing the distribution and sources of entropy generation on a local level. In a convective channel flow, the irreversibility arises due to the heat

* Corresponding author. Tel.: +39 081 5010217; fax: +39 081 5010204.
E-mail address: oronzio.manca@unina2.it (O. Manca).

0017-9310/$ - see front matter © 2006 Elsevier Ltd. All rights reserved.
doi:10.1016/j.ijheatmasstransfer.2006.01.032

Nomenclature

a	thermal diffusivity, m^2/s
b	channel gap, m
C_p	specific heat at constant pressure, J/(kg K)
Ec	Eckert number, Eq. (8)
g	acceleration due to the gravity, m/s^2
Gr	Grashof number, Eq. (5)
k	thermal conductivity, W/m K
L	channel plate height, m
L_x	height of the reservoir, m
L_y	width of the reservoir, m
Pr	Prandtl number, Eq. (5)
$\dot{q}$	heat flux, W/m^2
r^2	regression coefficient
Ra	Rayleigh number, Eq. (6)
T	temperature, K
T^*	dimensionless temperature, Eq. (8)
S'''	volumetric rate of entropy generation, $W/(m^3\ K)$
S^*	dimensionless volumetric entropy generation rate, Eq. (8)
$S^*_{X,Y}$	global entropy generation rate, Eq. (27)
u, v	velocity components along x, y, m/s
U, V	dimensionless velocities, Eq. (5)
x, y	cartesian coordinates, m
X, Y	dimensionless coordinates

Greek symbols

β	volumetric coefficient of expansion, 1/K
θ	dimensionless temperature, Eq. (5)
μ	dynamic viscosity, Pa s
ν	kinematic viscosity, m^2/s
ψ	stream function, m^2/s
Ψ	dimensionless stream function, Eq. (5)
ω	vorticity, 1/s
Ω	dimensionless vorticity, Eq. (5)

Subscript

∞	free stream condition

transfer as well as the viscous friction of the fluid. Theoretically, as long as the velocity and temperature gradients are known, the entropy generation at each point in the flow field can be calculated by means of the velocity and temperature data. Examples of calculation of local entropy production are reported in [16–23]. A numerical procedure for the prediction of local entropy rates was developed in [16] and it was applied to convective heat transfer in a jet impinging on a heated wall. The problem of entropy generation rates for mixed convection flows in a finned vertical channel was carried out in [17]. Evaluation of entropy generated in a conjugate heat transfer problem was obtained in [18]. The problem was the combined conduction–convection heat transfer due to a laminar confined planar impinging jet on a finite thickness plate. A numerical investigation for the evaluation of minimum entropy generation in natural convection in an inclined enclosure was accomplished in [19]. A two-dimensional laminar transient problem in stream-function-vorticity formulation, with Boussinesq approximation, was solved and local entropy generation was evaluated and presented in order to select the optimum inclination angle in terms of minimum entropy generation. Entropy generation in two-dimensional steady state laminar mixed convection from an isothermal rotating cylinder was carried out numerically in [20]. The results showed that the total generation entropy increased with the increase of both Reynolds number and buoyancy parameter but decreased with the increase of cylinder radius. Entropy generation calculations of two-dimensional laminar natural convection in an inclined cavity filled with saturated porous media was obtained by a numerical procedure in [21]. The local entropy generation maps were feasible and gave useful information for the selection of a suitable inclination angle. A numerical analysis of entropy generation in transient natural convection in a two-dimensional cavity with the two vertical surfaces at different temperatures was performed in [22]. Results showed that the total entropy generation presented a maximum value at the onset of the transient state. This maximum increased with the Rayleigh number and the irreversibility distribution ratio. Entropy generation, at steady state, was spread over the whole cavity at small Rayleigh numbers and was confined close to the active walls at high Rayleigh numbers. A numerical study of the effect of aspect ratio and surface waviness on heat transfer and entropy generation for natural convection in bent cavities was carried out in [23]. It was found that in conduction regime the irreversibility was dominated by the heat transfer. Increasing Rayleigh number the overall entropy generation was dominated by the fluid friction irreversibility. It seems to the authors' knowledge that the entropy generation analysis for natural convection in vertical channels has not been studied.

In this investigation, numerical behaviours of local and global entropy generation rates in natural convection in air in a vertical channel symmetrically heated at uniform heat flux are analyzed. Numerical solutions of the elliptic momentum and energy equations are carried out with the stream-function-vorticity method. Results of entropy generation analysis are obtained by solving the entropy generation equation based on the velocity and temperature data. The analyzed regime is two-dimensional, laminar and steady state. The numerical technique employed to discretize the equations is the control volume method on a uniform grid. Results are given in terms of entropy

generation fields and local entropy generation profiles, for various physical and geometrical parameters. Moreover, a correlation between global entropy generation values and significant parameters is given.

The usefulness of the entropy generation analysis in natural convection problems allows:

- to get an indication of the possible geometry modifications aimed to enhance the thermal performance of the system by means of local entropy production;
- to carry out a more complete thermal analysis of the considered configuration in order to compare this configuration with other similar geometries.

However, few complete thermal studies with an entropy generation analysis in natural convection have been proposed. Moreover, a numerical study about the entropy generation for natural convection in a vertical channel has not yet been considered.

2. Problem formulation

The configuration of the problem studied in this paper is depicted in Fig. 1(a). It is a vertical parallel plate channel; the parallel plates height is L whereas the channel gap is b. The channel walls are heated with a uniform heat flux equal to $\dot{q}$.

The flow is considered to be steady and laminar and the fluid properties are assumed to be constant except for the density in the buoyancy term of the momentum equation for the vertical direction, which is treated according to the Boussinesq approximation.

As described in [17], the expression for the volumetric rate of entropy generation is

$$S''' = \frac{k}{T^2}\left[\left(\frac{\partial T}{\partial x}\right)^2 + \left(\frac{\partial T}{\partial y}\right)^2\right] + \frac{\mu}{T}\left[2\left(\frac{\partial u}{\partial x}\right)^2 + 2\left(\frac{\partial v}{\partial y}\right)^2 + \left(\frac{\partial u}{\partial y} + \frac{\partial v}{\partial x}\right)^2\right] \quad (1)$$

By defining the dimensionless stream-function and vorticity as

$$U = \frac{\partial \Psi}{\partial Y}; \quad V = -\frac{\partial \Psi}{\partial X}; \quad \Omega = \frac{\partial V}{\partial X} - \frac{\partial U}{\partial Y}$$

the transformed governing equations, in dimensionless form, can be written in the following way:

$$\frac{\partial(U\Omega)}{\partial X} + \frac{\partial(V\Omega)}{\partial Y} = \nabla^2\Omega - Gr\frac{\partial \theta}{\partial Y} \quad (2)$$

$$\frac{\partial^2 \Psi}{\partial X^2} + \frac{\partial^2 \Psi}{\partial Y^2} = -\Omega \quad (3)$$

$$\frac{\partial(U\theta)}{\partial X} + \frac{\partial(V\theta)}{\partial Y} = \frac{1}{Pr}\nabla^2\theta \quad (4)$$

The dimensionless variables are:

$$X = \frac{x}{b}, \quad Y = \frac{y}{b}, \quad U = \frac{ub}{v}, \quad V = \frac{vb}{v}$$
$$\theta = \frac{(T - T_\infty)k}{\dot{q}b}, \quad \Psi = \frac{\psi}{v}, \quad \Omega = \frac{\omega b^2}{v}$$
$$Gr = \frac{g\beta\dot{q}b^4}{kv^2}, \quad Pr = \frac{v}{a} \quad (5)$$

The Rayleigh number is defined as:

$$Ra = GrPr \quad (6)$$

By following a similar non-dimensionalization procedure, the dimensionless form of the entropy generation equation is:

$$S^* = \frac{1}{(T^*)^2}\left[\left(\frac{\partial T^*}{\partial X}\right)^2 + \left(\frac{\partial T^*}{\partial Y}\right)^2\right] + \frac{PrEc}{T^*}\left[2\left(\frac{\partial U}{\partial X}\right)^2 + 2\left(\frac{\partial V}{\partial Y}\right)^2 + \left(\frac{\partial U}{\partial Y} + \frac{\partial V}{\partial X}\right)^2\right] \quad (7)$$

where

$$S^* = \frac{S'''b^2}{k}, \quad T^* = \left(\frac{\theta\dot{q}b}{kT_\infty} + 1\right) \quad \text{and} \quad Ec = \frac{(v/b)^2}{C_pT_\infty} \quad (8)$$

From a numerical point of view, an enlarged computational domain was chosen to simulate the free-stream conditions. The computational domain is made up of the simple vertical channel and two reservoirs of height L_x and width L_y, which are placed upstream and downstream of the channel. Due to thermofluidynamic and geometrical symmetries, the problem is solved in half domain, as shown in Fig. 1(b). The numerical solution of the thermal and dynamic fields was carried out as reported in [24]. The numerical solution of Eq. (7) has been carried out by employing the control volume method on a uniform grid

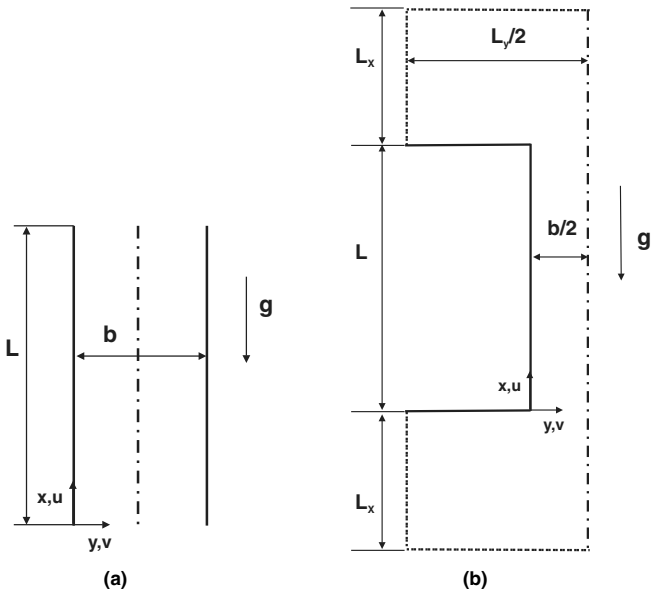

Fig. 1. Geometry of the problem: (a) physical configuration and (b) computational domain.

and a central scheme has been employed to discretize the various derivatives.

3. Analysis for fully developed case

In order to examine the behaviour of entropy production rate for lower Rayleigh number values, $Ra(b/L) < 0.14$, corresponding to the fully developed flow in laminar natural convection, the analytical solution of this motion is employed. Velocity and temperature profiles were carried out by [25] and their dimensionless form defined in Eqs. (5) is:

$$U = Gr\left[e^{\lambda Y/s}\left(c_1\cos\frac{\lambda Y}{s} + c_2\sin\frac{\lambda Y}{s}\right) + e^{-\lambda Y/s}\left(c_3\cos\frac{\lambda Y}{s} + c_4\sin\frac{\lambda Y}{s}\right)\right] \tag{9}$$

$$\theta = \frac{1}{Gr}\left[\alpha\left(X - \frac{L}{2b}\right) - \frac{d^2U}{dX^2}\right] \tag{10}$$

where $s = \sqrt{2}$, $\lambda = (\alpha Pr)^{1/4}$ with

$$\alpha = \frac{1}{0.1444}\left(\frac{b}{L}\frac{Gr}{Pr}\right)^{1/2} \tag{11}$$

The constants c_i $(i = 1,2,3,4)$ are:

$$c_1 = -\frac{c_2 e^{\lambda/s} + c_4 e^{-\lambda/s}}{e^{\lambda/s} - e^{-\lambda/s}}\tan\frac{\lambda}{s} \tag{12}$$

$$c_2 = \frac{-s - F_3\lambda^3 G}{\lambda^3(H - F_4 G)} \tag{13}$$

$$c_3 = -c_1 \tag{14}$$

$$c_4 = F_3 - c_2 F_4 \tag{15}$$

$$F_1 = \frac{\tan(\lambda/s)}{1 - e^{-\lambda s}} \tag{16}$$

$$F_2 = \frac{\tan(\lambda/s)}{e^{\lambda s} - 1} \tag{17}$$

$$F_3 = \frac{s}{\lambda^3(2F_2 + 1)} \tag{18}$$

$$F_4 = \frac{2F_1 + 1}{2F_2 + 1} \tag{19}$$

$$G = F_2 e^{\lambda/s}\left(\sin\frac{\lambda}{s} + \cos\frac{\lambda}{s}\right) + e^{-\lambda/s}\left(\sin\frac{\lambda}{s} + \cos\frac{\lambda}{s}\right) - F_2 e^{-\lambda/s}\left(\sin\frac{\lambda}{s} - \cos\frac{\lambda}{s}\right) \tag{20}$$

$$H = F_1 e^{\lambda/s}\left(\sin\frac{\lambda}{s} + \cos\frac{\lambda}{s}\right) + e^{\lambda/s}\left(\cos\frac{\lambda}{s} - \sin\frac{\lambda}{s}\right) - F_1 e^{-\lambda/s}\left(\sin\frac{\lambda}{s} - \cos\frac{\lambda}{s}\right) \tag{21}$$

For fully developed flows along the channel, at $Gr(b/L) \leqslant 0.20$, it results

$$V = 0 \quad \text{and} \quad \frac{\partial U}{\partial X} = 0 \tag{22}$$

and the dimensionless local entropy production, Eq. (6), is

$$S^* = \frac{1}{T^{*2}}\left[\left(\frac{\partial T^*}{\partial X}\right)^2 + \left(\frac{\partial T^*}{\partial Y}\right)^2\right] + \frac{Pr\,Ec}{T^{*2}}\left(\frac{dU}{dY}\right)^2 \tag{23}$$

with

$$\frac{\partial T^*}{\partial X} = \frac{\dot{q}b}{kT_\infty}\frac{\partial\theta}{\partial X} = \frac{\dot{q}b}{kT_\infty}\frac{\alpha X}{Gr} \tag{24}$$

$$\frac{\partial T^*}{\partial Y} = \frac{\dot{q}b}{kT_\infty}\frac{\partial\theta}{\partial Y} = -\frac{\dot{q}b}{kT_\infty}\frac{d^3U}{dY^3} \tag{25}$$

$$\frac{dU}{dY} = \frac{\lambda}{s}\left\{e^{\lambda Y/s}\left[(c_1 + c_2)\cos\frac{\lambda Y}{s} + (c_2 - c_1)\sin\frac{\lambda Y}{s}\right] + e^{-\lambda Y/s}\left[(c_4 - c_3)\cos\frac{\lambda Y}{s} - (c_3 + c_4)\sin\frac{\lambda Y}{s}\right]\right\} \tag{26}$$

The global entropy generation rate, S^*_{XY}, is obtained by integrating Eq. (23) with respect to X and Y coordinates

$$S^*_{X,Y} = \int_0^{L/b}\int_0^1 S^*(X,Y)\,dX\,dY \tag{27}$$

4. Results and discussion

Numerical results are presented in terms of entropy generation rates as local and over cross sections as global. The working fluid is air ($Pr = 0.71$), the channel aspect ratio, L/b, ranges between 5.0 and 20 and the Rayleigh number varies in the range $[10^3$–$10^6]$ for developing flows whereas for fully developed flows $Ra(b/L)$ is less than 0.14, as given by [25].

In Figs. 2 and 3, the distribution of local entropy generation rates is reported for $Ra = 10^3$ and 10^6 and for the aspect ratio equal to 5 and 10. In these figures the distributions are given inside and outside the heated channel. The extensions outside the channel are a small part of the two reservoirs.

Inside the channel, local distribution of entropy generation rates for $Ra = 10^3$, Fig. 2, presents curves at same entropy generation parallel to the channel walls, showing their minimum value along the centerline. This is due to the presence of thermal gradients along the channel transversal sections, which represent the highest contribute to the irreversibility. Moreover, the contour lines are parallel to each other because velocity and temperature profiles are fully developed at the lowest Rayleigh number value ($Ra = 10^3$). At the channel inlet ($X = 0$) and outlet ($X = L/b$) sections, it is observed that the isentropic lines are no more parallel to the channel plates. At the inlet section, they spread out and then they thicken close to the corner. In this reservoir zone, there are thermal gradients due to the presence of diffusive effects. At the channel inlet section, temperature differences between fluid and channel plates are present, too. These differences are highlighted by the elliptic numerical model employed in the momentum and energy equation solution. Moreover, for the reason given above, a field distortion close to the outlet zone is observed. In this zone there are the highest values of local entropy

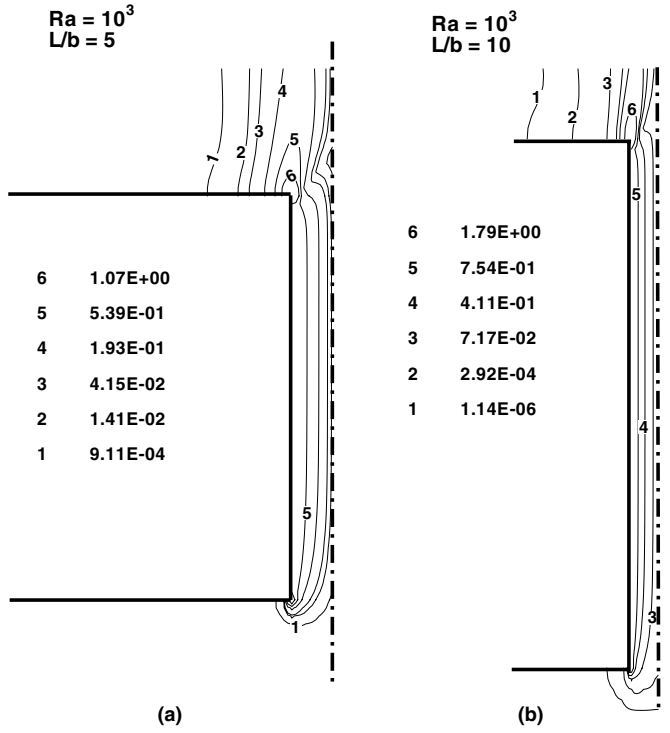

Fig. 2. Contours of normalized local entropy generation rate values at $Ra = 10^3$ with (a) $L/b = 5$ and (b) $L/b = 10$.

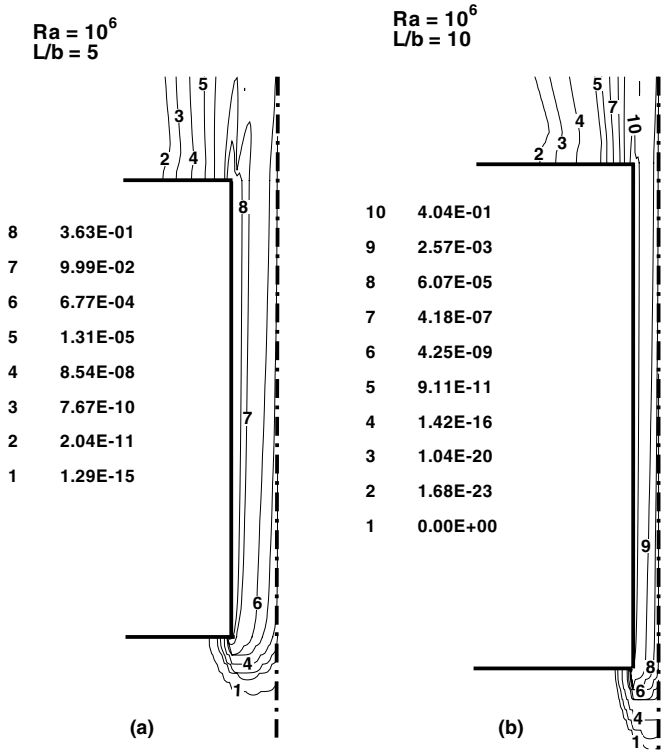

Fig. 3. Contours of normalized local entropy generation rate values at $Ra = 10^6$ with (a) $L/b = 5$ and (b) $L/b = 10$.

generation; these values are obtained at the corner. Entropy generation values not equal to zero are noticed in the upper reservoir due to the presence of thermal gradients. The effects are stronger for the configuration with $L/b = 5$, Fig. 2(a), than for the configuration analyzed in Fig. 2(b) ($L/b = 10$).

For the highest Rayleigh number value, Fig. 3, it is observed that the isolines are deviated towards the channel symmetry line. The deviation is as greater as lower the aspect ratio is, Fig. 3(a). This is due to the higher thermal gradients close to the channel plate and to the channel inlet because the boundary layer thickness is smaller at the highest Ra value ($Ra = 10^6$) and then velocity and thermal profiles are developing. It demonstrates that, at $Ra = 10^6$, thermal and dynamic fields are not completely developed. In Figs. 2 and 3, it has to be observed that local entropy generation values, as reported in the legend, are normalized by the corresponding maximum value attained inside the channel. In order to compare the values pertinent to different analyzed configurations, it is necessary to specify that these maximum values are: 5.35×10^{-8} at $Ra = 10^3$ and $L/b = 5$, 4.90×10^{-8} at $Ra = 10^3$ and $L/b = 10$, 6.07×10^{-2} at $Ra = 10^6$ and $L/b = 5$ and 6.19×10^{-2} at $Ra = 10^6$ and $L/b = 10$.

Normalized local entropy generation values as function of the transversal coordinate Y are reported in Figs. 4 and 5, for $Ra = 10^3$ and $Ra = 10^6$, respectively.

For $Ra = 10^3$ and $L/b = 5$, Fig. 4(a), it is observed that at the inlet section there is a strong local entropy generation decrease; in fact at $X = 0$, the local entropy generation passes from the maximum value equal to 1 at the channel wall to about 0.37 at $Y = 0.10$. So there is a decrease of 63% with respect to the maximum local entropy generation inside the channel whereas at $Y = 0.4$ local entropy generation values are close to zero. Increasing X, the area defined by the local entropy generation profile increases and at $X = 2.5$ it attains the greatest value among the three analyzed values. At $X = 2.5$, on the channel plate, the profile attains the minimum value, which is equal to 87% with respect to the maximum value whereas at $X = 5.0$, the minimum entropy generation value is 91% with respect to the maximum value. Close to the channel plate, the decrease along the cross section for $X = 2.5$ is lower than the one in the channel central zone. In fact, close to the channel plate, the local entropy generation values decrease up to 77% at $Y = 0.1$, up to 51% at $Y = 0.2$ and up to 26% at $Y = 0.3$. From $Y = 0.3$ the profile tends to a value close to zero. At $X = 5.0$ the profile shape is different with respect to the one at $X = 2.5$. The local entropy generation, referred to the maximum value, decreases more rapidly going from 91% at $Y = 0.0$ to 52% and 26% at $Y = 0.1$ and $Y = 0.2$, respectively.

For $L/b = 10$, Fig. 4(b), the local entropy generation decrease at the channel inlet is slightly slower than for the previous configuration for $L/b = 5$, varying from 1 at $Y = 0.0$ to 0.41 at $Y = 0.1$. The decrease is slightly slower at $X = 5.0$ and 10 than at the channel inlet, too.

For $Ra = 10^6$, Fig. 5, local entropy generation tends to zero at all the analyzed cross sections. This confirms that

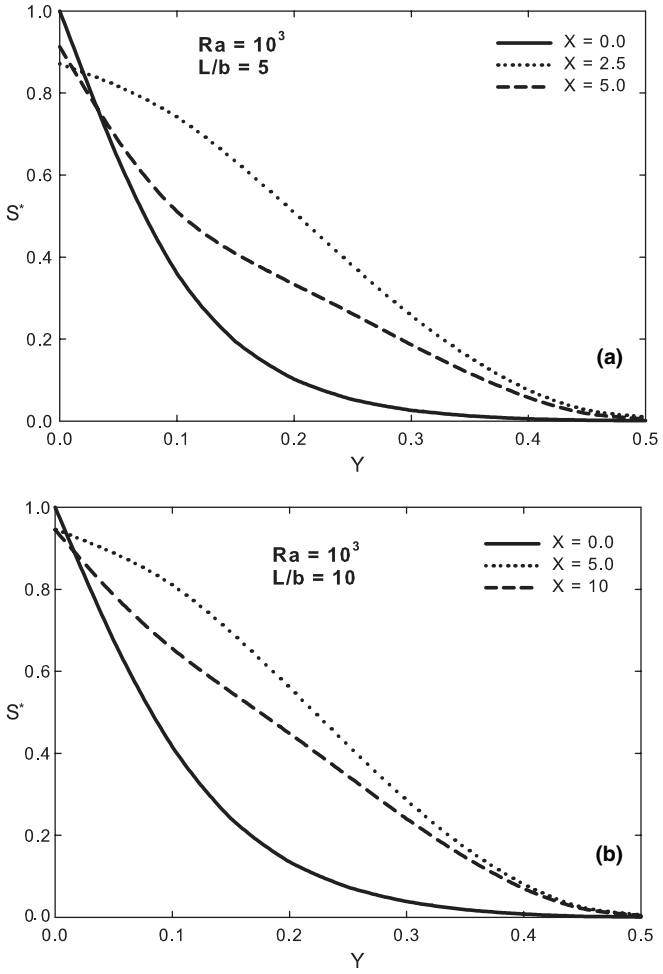

Fig. 4. Normalized local entropy generation rate profiles at $Ra = 10^3$ with (a) $L/b = 5$ and (b) $L/b = 10$.

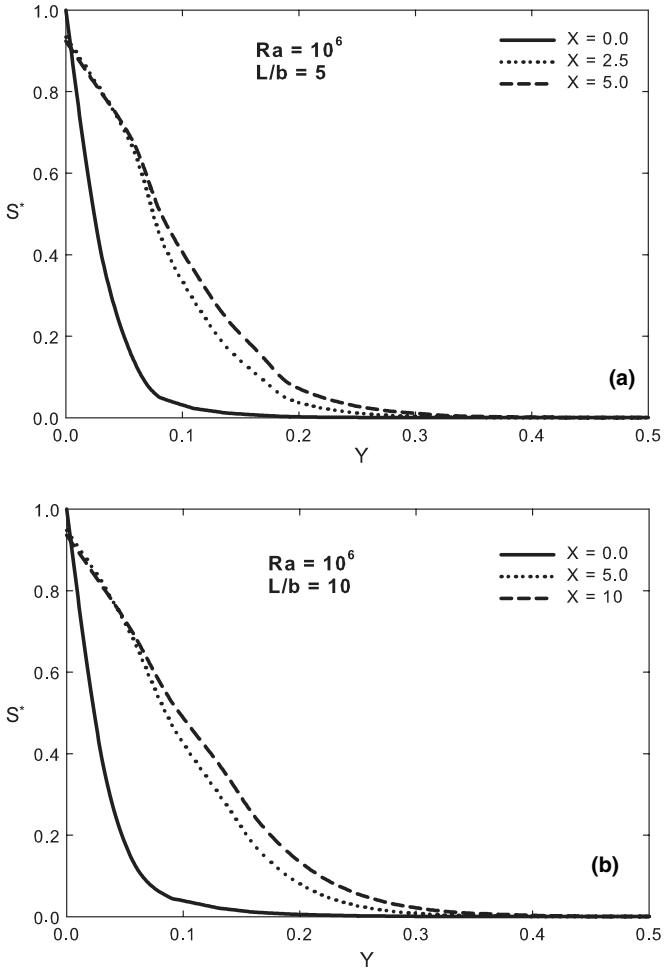

Fig. 5. Normalized local entropy generation rate profiles at $Ra = 10^6$ with (a) $L/b = 5$ and (b) $L/b = 10$.

the more disturbed zone has a lower thickness at this Ra value than the one corresponding to $Ra = 10^3$, for the same L/b value. For $L/b = 5$, Fig. 5(a), at the inlet section, the local entropy generation value varies from 1.0 at the channel wall to 0.18 at $Y = 0.1$ and about 0 at $Y = 0.3$. At the sections $X = 2.5$ and 5.0, the values at the channel walls are 0.93 and 0.92, respectively so as at $Y = 0.05$ where they assume very similar values, approximately equal to 0.70. They become negligible at $Y = 0.3$. For $L/b = 10$, Fig. 5(b), the profiles attain values slightly higher than in the previous case ($L/b = 5$). In fact, at $Y = 0.0$ the local entropy generation value is equal to 0.95 at $X = 5.0$ and 0.94 at the channel outlet. At both $X = 5.0$ and 10, the value is 0.72 at $Y = 0.05$, whereas at $Y = 0.10$ the values are 0.43 at $X = 5.0$ and 0.48 at $X = 10$.

Local entropy production profiles, S^*, for $Ra = 1.42$ and 2.84 with $L/b = 20$, corresponding to the fully developed laminar natural convection condition, are reported in Fig. 6. For these Ra values the entropy generation rate profiles along the transversal section are developed and the variation along the X coordinate is negligible. For this reason only one profile is shown for assigned Rayleigh

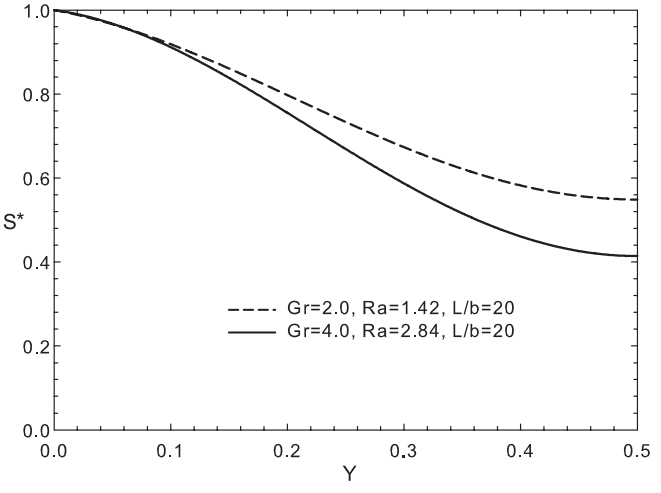

Fig. 6. Normalized local entropy production rate profiles for fully developed flow at $L/b = 20$ for $Ra = 1.42$ and 2.84.

number. It is observed in Fig. 6 that the slope of the curves close to the wall, $Y < 0.1$, increases slightly and for $Y > 0.2$ the slope decreases. The maximum value is on the wall,

Table 1
Global entropy generation rate vs Rayleigh number and aspect ratio

Ra	$L/b = 5$	$L/b = 10$	$L/b = 15$	$L/b = 20$
10^3	6.10×10^{-8}	1.27×10^{-7}	1.83×10^{-7}	2.49×10^{-7}
10^4	4.99×10^{-6}	1.06×10^{-5}	1.64×10^{-5}	2.25×10^{-5}
10^5	3.68×10^{-4}	8.15×10^{-3}	1.30×10^{-3}	1.88×10^{-3}
10^6	2.87×10^{-2}	6.74×10^{-1}	1.12×10^{-1}	1.53×10^{-1}

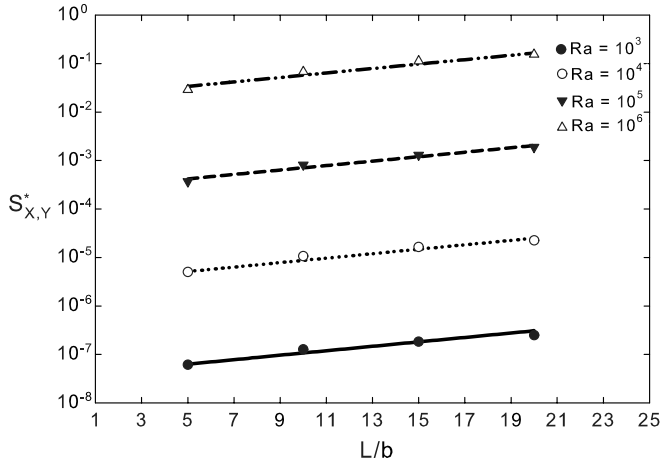

Fig. 7. Comparison between numerical and predicted global entropy generation rate values inside the channel, for the investigated configurations.

where temperature and velocity gradients reach the maximum values. At $Y = 0.50$ the local entropy production rate is about 40% and 55% of the maximum value for $Ra = 1.42$ and 2.84, respectively.

Global entropy generation values for the different analyzed cases are reported in Table 1. It is to be noticed that the global entropy generation increases with both aspect ratio and Rayleigh number increase. Global entropy generation changes significantly with respect to the Rayleigh number. These values have been correlated as function of Ra and L/b; the correlation obtained by means of the least square method is

$$\log S^*_{X,Y} = -13.2 + 1.91 \log Ra + 0.045(L/b) \quad (28)$$

with $r^2 = 0.999$, $5 \leqslant L/b \leqslant 20$, $10^3 \leqslant Ra \leqslant 10^6$.

In Fig. 7 the proposed correlation in Eq. (28) and the employed numerical data as a function of the channel aspect ratio, L/b, for different Ra values, are reported. A very good agreement between the equation and the numerical data is observed.

5. Conclusions

The evaluation of the entropy production rates in natural convection in air in a vertical channel symmetrically heated was carried out numerically by means of a computational procedure. The numerical procedure expanded an existing computer code on natural convection. Moreover, the evaluation of the entropy production rates was carried out also for the fully developed limit.

Local and global entropy generation rates in terms of Rayleigh number, Ra, and aspect ratio values, L/b, were given. The distribution of local values showed different behaviours for the different Ra values. At $Ra = 10^3$ the lines at constant entropy generation were parallel to the channel walls whereas they were slightly inclined toward the centerline at $Ra = 10^6$. In both cases the highest local values were on the corner at the outlet section. At the channel inlet section, the profiles showed local values going to zero more rapidly. This effect was stronger at the higher Rayleigh number values. According to the fully developed flow results also the entropy production rates presented fully developed profiles.

Global entropy generation rates increased as both the aspect ratio increased and the Rayleigh number increased. The decrease with respect to L/b was lower than that with respect to Ra value. A correlation among the global entropy generation rates, Ra and L/b was proposed in the ranges $5 \leqslant L/b \leqslant 20$, $10^3 \leqslant Ra \leqslant 10^6$. A very good agreement was obtained between the equation and numerical data.

Acknowledgements

This research is funded by the PRIN 2005 and SUN 2003 and 2005.

References

[1] A. Bejan, A study of entropy generation in fundamental convective heat transfer, J. Heat Transfer 101 (1979) 718–725.
[2] A. Bejan, Entropy Generation Minimization, CRC Press, Boca Raton, FL, 1996.
[3] A. Bejan, Shape and Structure from Engineering to Nature, Cambridge University Press, New York, 2000.
[4] V.D. Zimparov, N.L. Vulchanov, Performance evaluation criteria for enhanced heat transfer surfaces, Int. J. Heat Mass Transfer 37 (1994) 1807–1816.
[5] A. Bejan, G.A. Ledezma, Thermodynamic optimization of cooling techniques for electronic packages, Int. J. Heat Mass Transfer 39 (1996) 1213–1221.
[6] L. Tagliafico, G. Tanda, A thermodynamic method for the comparison of plate-fin heat exchanger performance, J. Heat Transfer 118 (1996) 805–809.
[7] W.W. Lin, D.J. Lee, Second law analysis on a pin-fin array under crossflow, Int. J. Heat Mass Transfer 40 (1997) 1937–1945.
[8] D.P. Sekulic, A. Campo, J.C. Morales, Irreversibility phenomena associated with heat transfer and fluid friction in laminar flows through singly connected ducts, Int. J. Heat Mass Transfer 40 (1997) 905–914.
[9] A.Z. Sahin, Second law analysis of laminar viscous flow through a duct subjected to constant wall temperature, J. Heat Transfer 120 (1998) 76–83.
[10] J. Cervantes, F. Solorio, Entropy generation in a plane turbulent oscillating jet, Int. J. Heat Mass Transfer 45 (2002) 3125–3129.
[11] S. Mahmud, R.A. Fraser, Analysis of mixed convection–radiation interaction in a vertical channel: entropy generation, Exergy 2 (2002) 330–339.

[12] G. Ibez, S. Cuevas, M. Lopez de Haro, Minimization of entropy generation by asymmetric convective cooling, Int. J. Heat Mass Transfer 46 (2003) 1321–1328.
[13] S. Mahmud, R.A. Fraser, The second law analysis in fundamental convective heat transfer problems, Int. J. Thermal Sci. 42 (2003) 177–186.
[14] O.B. Adeyinka, G.F. Naterer, Optimization correlation for entropy production and energy availability in film condensation, Int. Commun. Heat Mass Transfer 31 (2004) 513–524.
[15] S. Mahmud, R.A. Fraser, Flow, thermal, and entropy generation characteristics inside a porous channel with viscous dissipation, Int. J. Thermal Sci. 44 (2005) 21–32.
[16] M.K. Dorst, M.D. White, Numerical predictions of local entropy generation in an impinging jet, J. Heat Transfer 113 (1991) 823–829.
[17] C.H. Cheng, W.P. Ma, W.H. Huang, Numerical predictions of entropy generation for mixed convective flows in a vertical channel with transverse fin array, Int. Commun. Heat Mass Transfer 21 (1994) 519–530.
[18] G. Ruocco, Entropy generation in conjugate heat transfer from a discretely heated plate to an impinging confined jet, Int. Commun. Heat Mass Transfer 24 (1997) 201–210.
[19] A.C. Baytas, Optimization in an inclined enclosure for minimum entropy generation in natural convection, J. Non-Equilib. Thermodyn. 22 (1997) 145–155.
[20] B.A.K. Abu-Hijleh, W.N. Heilen, Entropy generation due to laminar natural convection over a heated rotating cylinder, Int. J. Heat Mass Transfer 42 (1999) 4225–4233.
[21] A.C. Baytas, Entropy generation for natural convection in an inclined porous cavity, Int. J. Heat Mass Transfer 43 (2000) 2089–2099.
[22] M. Magherbi, H. Abbassi, A. Ben Brahim, Entropy generation at the onset of natural convection, Int. J. Heat Mass Transfer 46 (2003) 3441–3450.
[23] S. Mahmud, R.A. Fraser, Free convection and entropy generation inside a vertical inphase wavy cavity, Int. Commun. Heat Mass Transfer 31 (2004) 455–466.
[24] A. Andreozzi, O. Manca, Thermal and fluid dynamic behaviour of symmetrically heated vertical channels with auxiliary plate, Int. J. Heat Fluid Flow 22 (2001) 424–432.
[25] W. Aung, Fully developed laminar free convection between vertical plates heated asymmetrically, Int. J. Heat Mass Transfer 15 (1972) 1577–1580.